Taylor & Francis
Taylor & Francis Group

Ship Technology Research
Schiffstechnik

ISSN: 0937-7255 (Print) 2056-7111 (Online) Journal homepage: www.tandfonline.com/journals/ystr20

Rudder force calculation in the early design stage considering propeller–rudder interaction

Björn Carstensen

To cite this article: Björn Carstensen (31 Jul 2025): Rudder force calculation in the early design stage considering propeller–rudder interaction, Ship Technology Research, DOI: 10.1080/09377255.2025.2537538

To link to this article: https://doi.org/10.1080/09377255.2025.2537538

Published online: 31 Jul 2025.

SHIP TECHNOLOGY RESEARCH (SCHIFFSTECHNIK)
https://doi.org/10.1080/09377255.2025.2537538

Rudder force calculation in the early design stage considering propeller–rudder interaction

Björn Carstensen *

Institute of Ship Design and Ship Safety, Hamburg University of Technology (TUHH), Hamburg, Germany

ABSTRACT

Due to the growing requirements on energy efficiency of ships, certain problems and challenges arise for the design of rudders and propellers. For the rudder, the focus changes for many ship types from solely being a manoeuvring device to positively influencing the propulsion. This paper summarizes a hybrid calculation method for the calculation of rudder forces and for the evaluation of the bidirectional interaction between propeller and rudder for the early design stage. The new hybrid calculation method couples a lifting line approach for multi-component-propulsors with a panel method and a two-dimensional boundary layer method. The calculation results of the developed method are validated with measurements from several model tests. Finally, an application for full-scale predictions is presented.

ARTICLE HISTORY
Received 21 March 2025
Accepted 17 July 2025

KEYWORDS
Propeller–rudder–interaction; lifting line; boundary element method; boundary layer method; hybrid calculation method

1. Introduction

This paper is a summary of the author's German PhD thesis (Carstensen 2023), for which he was awarded the Curt Bartsch Award 2024.

The hydrodynamic performance of a rudder influences several aspects of a ship design. First, the rudder influences the manoeuvring performance of the vessel, as the rudder is the main manoeuvring device in a conventional arrangement. But apart from that, the rudder influences also the resistance of the vessel. While the resistance of the rudder straight ahead is almost negligible small, it grows to a share of 2%–6% of the calm water resistance when used for course keeping in real operation (Alte and vom Baur 1986). Furthermore, the rudder indirectly influences the resistance due to drift, which is for common drift angles in the range of 5%–25% of the calm water resistance (Kringel 1974; Wagner 1974). The drift angle can be lowered by a beneficial rudder design and therefore also the corresponding resistance of the drifting ship.

While the rudder was formerly mainly investigated regarding its manoeuvring performance, the focus shifts due to stricter regulations (Marine Environment Protection Committee 2011, 2018, 2021) and a strong competition in the market to the aspect of the efficiency. For the assessment of the manoeuvring performance in the early design stage, several well-proven approaches exist. But when taking the aspect of the energy efficiency into account, there is a lack of methods that can be applied in the early design stage. The requirements of a method for rudder force calculation in the early design stage are:

- low computation and modelling time,
- possible application for a yard and a rudder manufacturer,
- limited input data from the early design stage,
- calculation of rudder forces and moments for numerous operating conditions as input for manoeuvring simulations,
- high accuracy for the rudder forces, especially for the drag,
- inclusion of the bidirectional propeller–rudder interaction,
- calculation of the separation behaviour in model and in full scale.

This paper presents a newly developed, validated hybrid method for this purpose fulfilling the above-mentioned requirements.

2. Hybrid method

The developed method consists of three parts forming a hybrid coupled method. The aim of the suitable combination is increasing the accuracy and counteracting the met simplifications without significantly increasing the calculation effort. Each individual part

CONTACT Björn Carstensen carstensen@hsva.de
*Current address: The Hamburg Ship Model Basin (HSVA) in Hamburg, Germany.

of the hybrid method is shortly outlined in the following subsections, without pretence to describe every detail. As the underlying theory and their solution is very extensive, the details can be found in the corresponding literature. The coupling of all parts of the hybrid method is covered in the last subsection.

2.1. Lifting line theory

The lifting line method used here for the propeller is described by Isay (1964) and was adapted to modern propeller geometries by Krüger and Abels (2017). When extending the lifting line approach to the propeller–rudder arrangement, the underlying mathematical problem becomes a double simultaneous boundary value problem (see Isay 1970, p. 67 ff.). To solve this problem, Isay (1970) suggests an iterative approach, which is implemented by Krüger (2019) for common arrangements of multi-component-propulsors, as e.g. pre-swirl and post-swirl devices in combination with a propeller or contra-rotating propellers. The bidirectional interaction between the involved propulsors is handled by the induced velocities of each component at all other components. Krüger (2019) calculates these induced velocities by extending the Goldstein factors (Goldstein 1929) from literature (Lerbs 1955) for one to eight bladed propulsors for very low and very high pitch of the free vortex system. Furthermore, induction factors, like Lerbs (1955), are calculated for the aforementioned cases.

2.2. Boundary layer method

To capture viscous effects within the otherwise potential methods, a two-dimensional integral boundary layer method is added to the hybrid method. To solve the laminar part of the flow, the momentum equation is solved using the velocity profile perpendicular to the surface of von Kármán (1921) and Pohlhausen (1921) with the extension of Marzi (1988) for positive pressure gradients. This approach leads to an inhomogeneous differential equation, which can be solved as initial value problem in the stagnation point. The values downstream can then be calculated by integration.

The location of the transition from laminar to turbulent is calculated with the modified e^N approach of Krüger (1992). At the point of transition, the laminar solution becomes unstable. To find this point, an interference is superimposed to the initial laminar solution, which leads to the Orr–Sommerfeld equation (Orr 1907; Sommerfeld 1908).

In a simplified manner, it is assumed in this boundary layer method that the flow is instantaneous turbulent from the point of transition. The turbulent part of the flow is calculated by solving two simultaneous differential equations described by Gruschwitz (1931). One of the equations describes the form parameter, which is the ratio between the thickness of the boundary layer and the momentum loss thickness, and the other one describes the non-dimensional momentum loss thickness.

Finally, the drag of a section is calculated from the loss of momentum by the equations given by Squire and Young (1937). This is done by extrapolating the results of the boundary layer calculation at the trailing edge to infinity. The calculated drag includes the skin friction and the viscous pressure loss.

2.3. Panel method

A panel method is used for the calculation of the flow field around the rudder and subsequent analysis as e.g. forces, moments and pressure distributions. The used method is a three-dimensional, desingularized, direct panel method (Söding 1997). The desingularization is achieved by placing the collocation points inside the body, while the body is discretized by constant surface sources and dipoles. The strength of the dipoles on the wake panels is taken implicit from the potential difference at the trailing edge.

This simplification at the trailing edge linearizes the flow problem. For wings with small aspect ratio, the linearization does no longer hold, as the pronounced tip vortex leads to non-linearities at high angles of attack. The aspect ratio of a rudder typically falls into the range of this non-linearity. To achieve accurate results, the panel method is extended by a semi-empirical approach, in which the strength of the circulation of the free vortices is iteratively adjusted to fulfil the third theorem of Helmholtz at the location of the tip vortices.

For the subsequently presented coupling of the three-dimensional panel method with a boundary layer method, trajectories on the surface of the rudder need to be derived. Along these trajectories, a high accuracy is needed for the velocity and the pressure distribution. The direct calculation of trajectories from the results of the panel methods holds

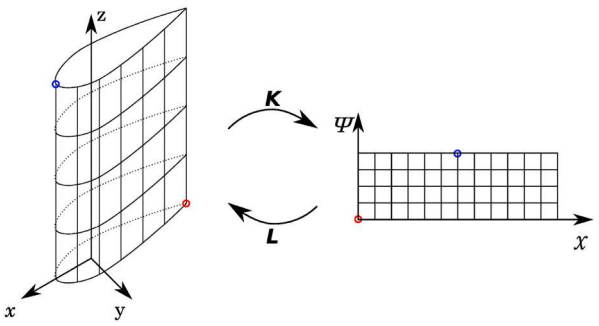

Figure 1. Coordinate system and grid of the physical space (left) and the computational space (right) with the corresponding transformations. Two exemplary transformed points are highlighted as red and blue dots.

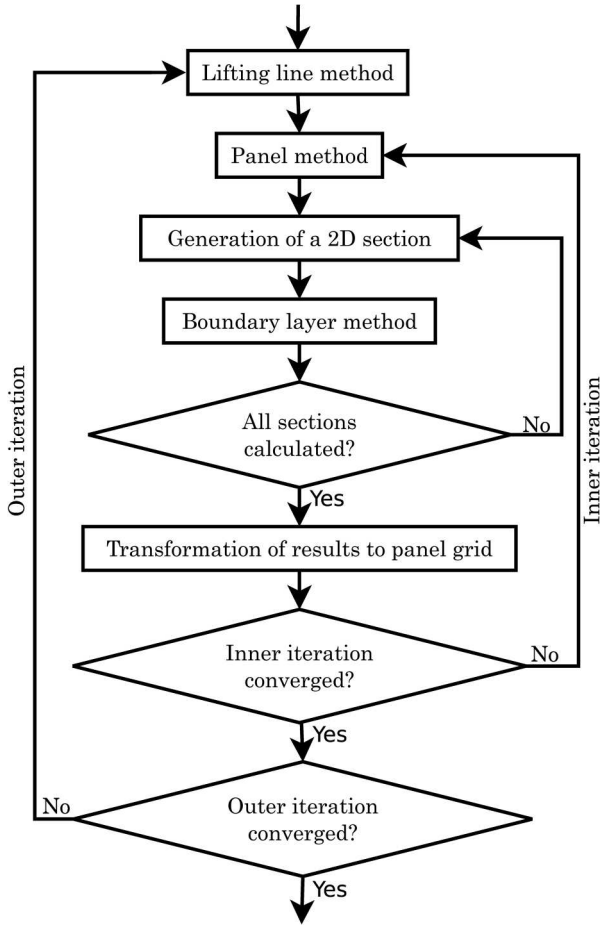

Figure 2. Schematic flowchart of the coupled hybrid method.

difficulties, due to high curvature near the leading edge (and therefore near the stagnation point) and due to a coarse discretization of the surface. To solve these difficulties, the three-dimensional results of the panel method are transformed from the so-called physical space to a two-dimensional rectangular uniform grid (computational space), which is shown in Figure 1. The approach extends the work of Zingg and Yarrow (1989). Their approach is limited to a transformation within two two-dimensional grids. By transforming the results from the three-dimensional domain to a two-dimensional grid, the calculation simplifies strongly, and the velocities stay automatically on the surface. The transformation matrices only depend on geometrical attributes and can therefore be precomputed during grid generation.

2.4. Coupled hybrid method

The present application case cannot sufficiently be solved solely by a classic panel method, as the equation system would become singular when the wake panels of the propeller penetrate the rudder surface. Another difficult task is the rudder wake alignment, which needs to be covered thoroughly for high accuracy in the results. And finally, the panel method is not capable to calculate viscous effect due to the met simplifications of the potential theory.

In order to solve these problems, the previously outlined methods are coupled in a hybrid method for the rudder force calculation with consideration of the propeller–rudder interaction. Details of the coupling are given in Carstensen and Krüger (2021) and Carstensen (2021, 2023). The approach is schematically shown as a flow chart in Figure 2.

In the coupled hybrid method, the lifting line method (see Section 2.1) is executed at the beginning. It delivers very fast first estimations for the flow field, which is then used as inflow in the panel method. Moreover, the flow field is used for the wake alignment of the wake panels in the panel method (see Carstensen 2021). As shown in Figure 3, the flow field is separated into the flat contribution from the rudder angle and the rotatory contribution from the propeller forming together the deformed complex geometry of the wake panels. Furthermore, the forces and moments on the propeller are calculated within the lifting line method.

Afterwards, the panel method (see Section 2.3) is executed. It builds the core of the hybrid method and is used for the calculation of the forces on and the flow around the rudder.

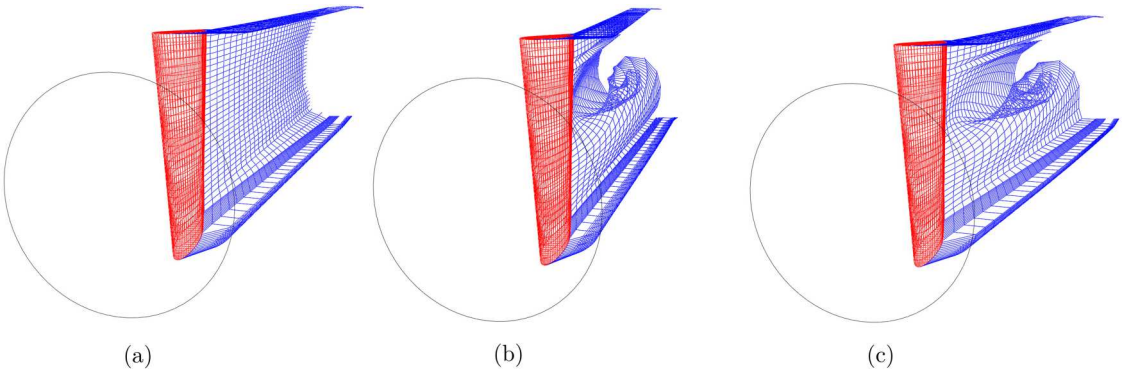

Figure 3. Visualization of different contributions to the deformation of the wake field of an exemplary full spade rudder behind a propeller. (a) Flat contribution from rudder angle in homogeneous inflow. (b) Rotatory contribution from exemplary propeller inflow. (c) Combined full wake geometry.

The boundary layer method (see Section 2.2) is executed after the panel method. The results of the boundary layer deliver insights into the viscous effects as for example the separation behaviour, or the viscous drag. As described in Section 2.3, two-dimensional sections need to be calculated to use these as input for the boundary layer method. One implemented approach are the previously discussed trajectories on the surface of the rudder. There is also an approach of profiles (horizontal rudder sections) implemented, which is more robust, but also less accurate. The second approach will not be further dealt with in this paper. Several sections are calculated so that the three-dimensional geometry of the rudder is sufficiently covered. The direct results from the boundary layer method are the viscous drag of a section and the boundary flow and separation behaviour. To take the thickness of the boundary layer into account in the panel method, the so-called transpiration velocity of Lighthill (1958) is applied.

The boundary layer method and the panel method are run through in an inner iteration. Afterwards, the induced velocities in the propeller plane and the correct rudder circulation derived from the inner iteration, are handed back to the lifting line method. This loop back is the outer iteration. In standard applications, the outer and inner iteration each converge after two to three iteration steps.

3. Validation

The underlying author's PhD thesis (Carstensen 2023) validates the method with four different model test setups. Each of the validation setups covers different aspects of the method. In this paper, only a limited scope of these validations is presented in the following subsections.

3.1. Rudder in homogenous inflow

For the rudder in homogeneous inflow, the developed method is validated with the model tests of Molland and Turnock (1991, p. 37) and Molland and Turnock (1993, p. 25). The main particulars of the rudder are given in Table 1. The model tests were carried out in a wind tunnel with a symmetric rudder with inflow speeds between $u_\infty = 20\,\mathrm{m\,s^{-1}}$ and $u_\infty = 25\,\mathrm{m\,s^{-1}}$ leading to Reynolds numbers on the rudder between $Re = 0.8 \times 10^6$ and 1×10^6. The experimental setup is schematic shown in Figure 4.

Table 1. Geometric parameters of the rudder from model tests of Molland and Turnock (2007, p. 125–182).

Model		Ruder 2
Span h	[m]	1.000
Mean chord length $\bar{c}$	[m]	0.667
Rudder area A_{Rud}	[m^2]	0.667
Geom. aspect ratio Λ	[–]	1.500
Sweep Ω	[°]	0
Taper λ_R	[°]	0
Profile family		NACA 4
Rel. thickness root (t/c)W	[–]	0.200
Rel. thickness tip (t/c)S	[–]	0.200

The forces of the model tests are compared to the results of the developed method in non-dimensional form in Figure 5. These are made non-dimensional as follows:

$$c_F = \frac{F}{0.5\rho u_\infty^2 A_{\mathrm{Rud}}}, \tag{1}$$

where the force is denoted as F, the inflow velocity as u_∞ and the area of the rudder as A_{Rud}. The lift force in Figure 5 calculated by the hybrid calculation method is in good agreement with the two measurement series. The calculation slightly overestimates the lift, which is also reported by other authors in their calculations (Turnock 1993; Simonsen 2000). Reasons for this may be the boundary layer of the wind tunnel and mirror effects of the closed wind tunnel.

In Figure 5, each point depicts a measurement or calculation point. With red dots are points marked, where flow separation occurs in the boundary layer calculation. At approximately $\pm 20°$ rudder angle, where flow separation is predicted, is in a very good agreement with the spontaneous drop of the lift force in the measurements. The developed method cannot be used for cases with flow separation. Therefore, the lift is overestimated after the occurrence of flow separation. The drag force also corresponds well with the measurements in the region of attached flow ($\|\delta_R\| < 20°$).

3.2. Rudder behind propeller

The arrangement of a rudder behind a propeller is validated using two model tests for the same vessel.

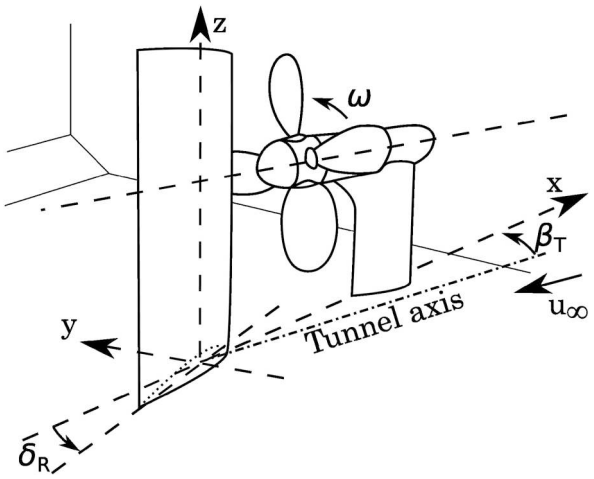

Figure 4. Schematic experimental setup in model tests of Molland and Turnock (2007, p. 125-182) in own presentation according to Molland and Turnock (2007, p. 130).

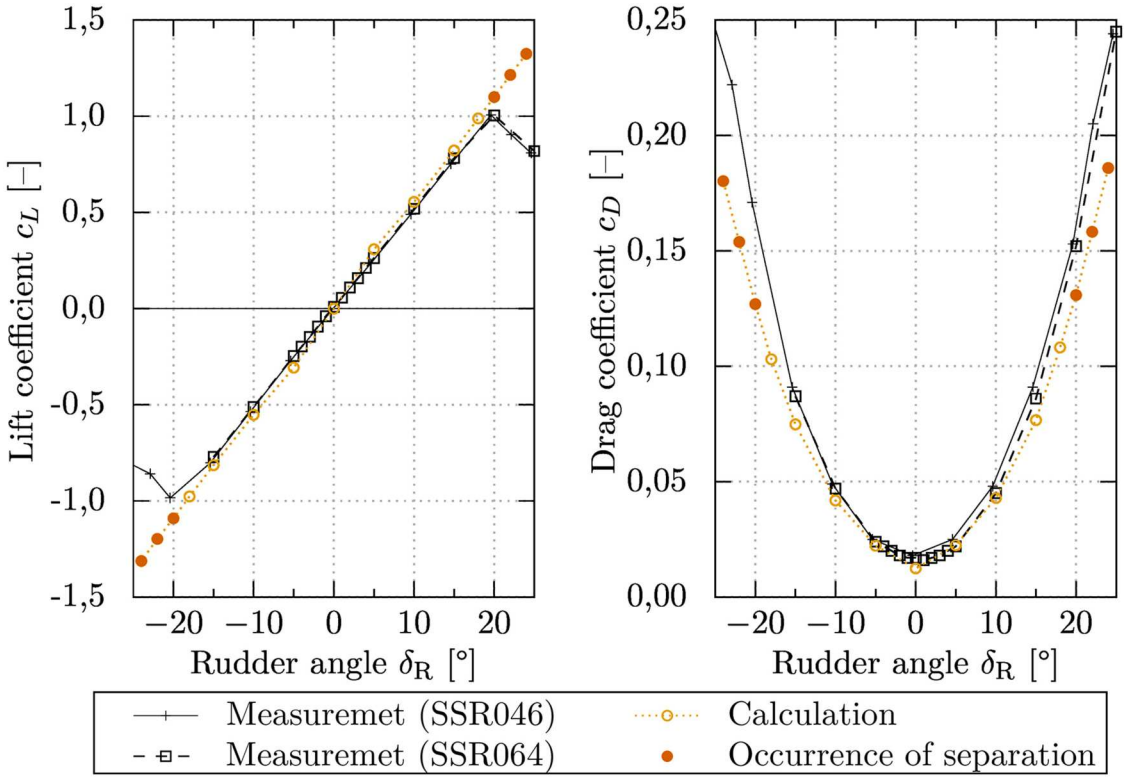

Figure 5. Comparison of forces between measurements (Molland and Turnock 1991, 1993) and calculations for rudder No. 2 in homogeneous inflow.

One was carried out by Wolf (1997) in a circulating water tank and the other are resistance and propulsion tests with rudder force measurements of Günther and Röpcke (1996). In the circulating water tank, only propeller and rudder were present without the ship hull. The arrangement is schematically drawn in Figure 6(a). Rudder angle of $\delta_R = -45$ to $45°$ were investigated at different propeller thrust loadings. The test setup during resistance and propulsion tests was a standard setup with additional rudder force measurement, which is shown in Figure 6(b). The rudder angle was varied between $\delta_R = -40$ to $40°$ at constant maximum power and therefore variable speed. Both tests setups were carried out with the same symmetric rudder and propeller. The geometric parameters of the rudder in models and in full scale are given in Table 2. Apart from the two different model tests, calculations were carried out for this case by Söding (1997) using a potential panel method.

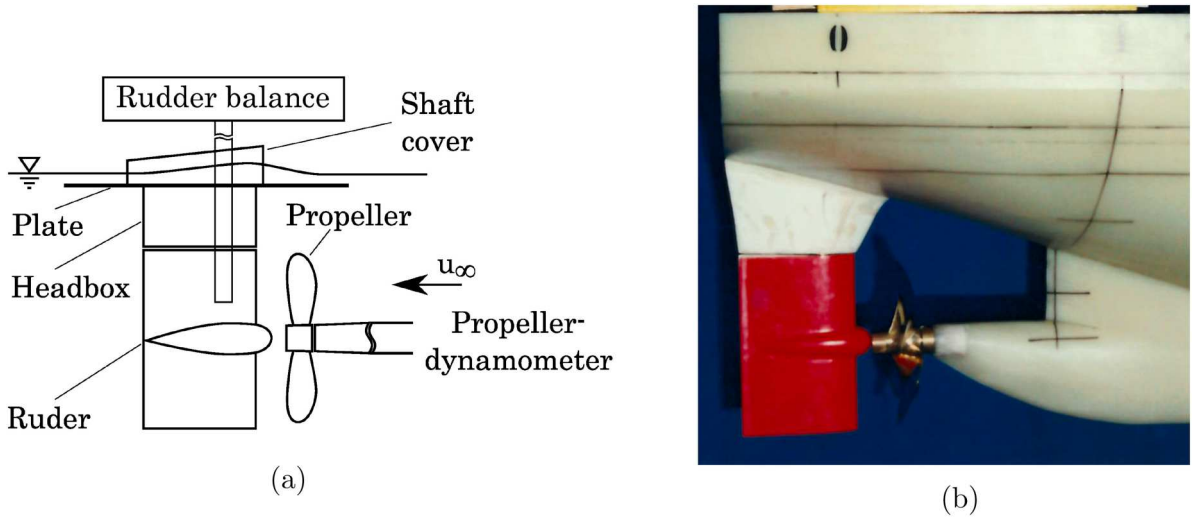

Figure 6. Experimental setups in model tests of the validation case for rudder behind propeller configuration. (a) Schematic experimental setup in model tests of Wolf (1997) in own presentation according to Wolf (1997, p. 8). (b) Experimental setup in model tests of Günther and Röpcke (1996, p. 4.2).

Table 2. Geometric parameters of the rudder from model tests of Wolf (1997) and Günther and Röpcke (1996).

	Model	Full scale
Scale λ_M	24.1070	–
Span h_M	0.2364 m	5.6989 m
Mean chord length $\bar{c}_M$	0.1478 m	3.5630 m
Rudder area A_{Rud}	0.0349 m^2	20.2820 m^2
Geom. aspect ratio Λ	1.6000	
Sweep Ω	0°	
Taper λ_R	0	
Profile family	HSVA MP 73	
Rel. thickness root $(t/c)_W$	0.2500	
Rel. thickness tip $(t/c)_S$	0.1800	

The non-dimensional rudder forces and moments are compared between the two measurements, the values from literature and the hybrid method in Figure 7. As the homogeneous inflow cannot be used in or near bollard pull and as it is difficult to define an inflow velocity in the inhomogeneous flow behind a propeller, the forces are made non-dimensional using propeller particulars:

$$k_F = \frac{F}{\rho n^2 D_P^4}, \tag{2}$$

with F being the force that should be made non-dimensional, the density ρ, n the propeller revolutions and the propeller diameter D_P. Moments are made non-dimensional in the same manner:

$$k_M = \frac{M}{\rho n^2 D_P^5}, \tag{3}$$

while M denotes the moment that should be made non-dimensional.

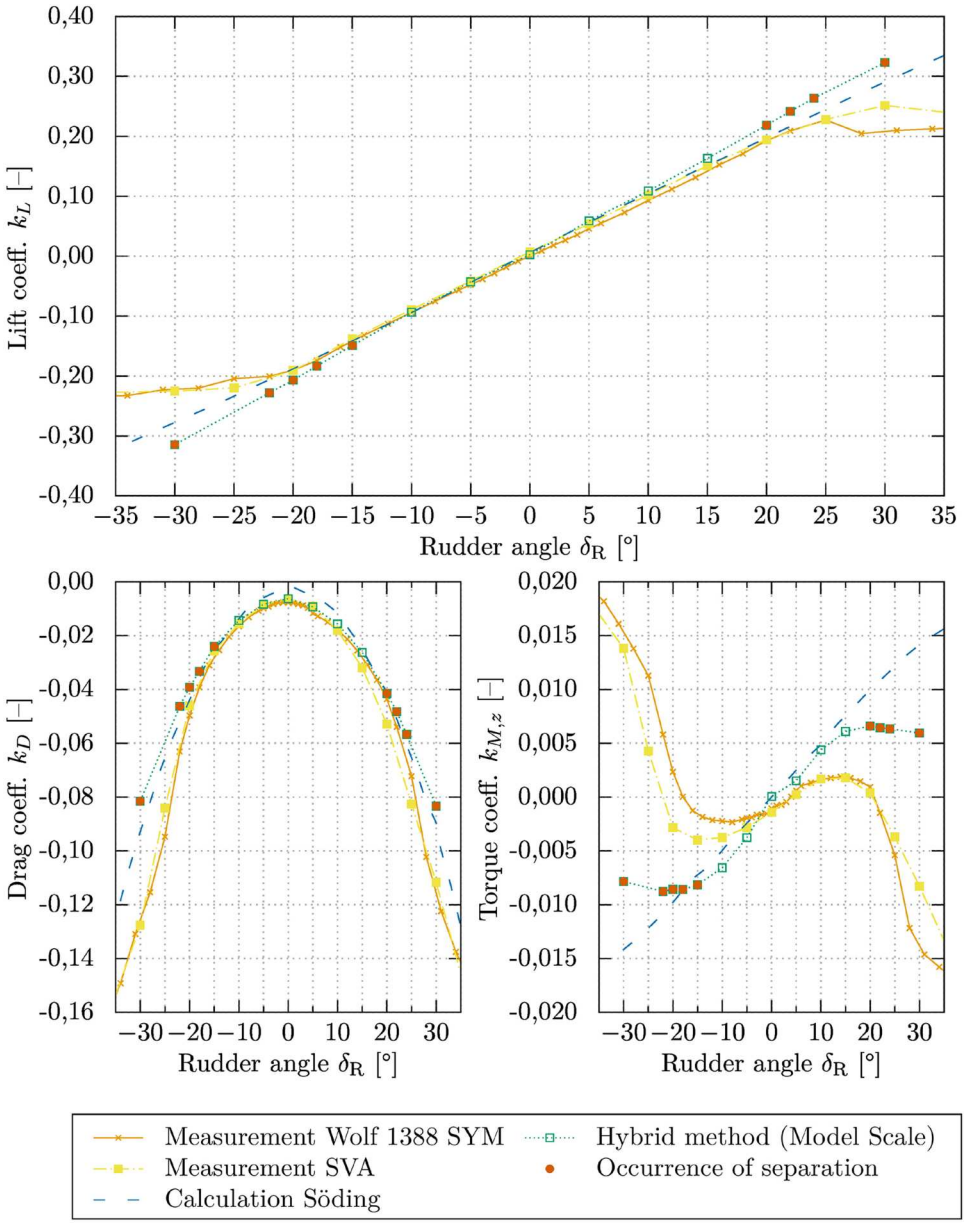

Figure 7. Comparison of rudder forces and torque between calculations with the hybrid method, calculations of Söding (1997), measurements of SVA (Günther and Röpcke 1996) and measurements of Wolf (1997).

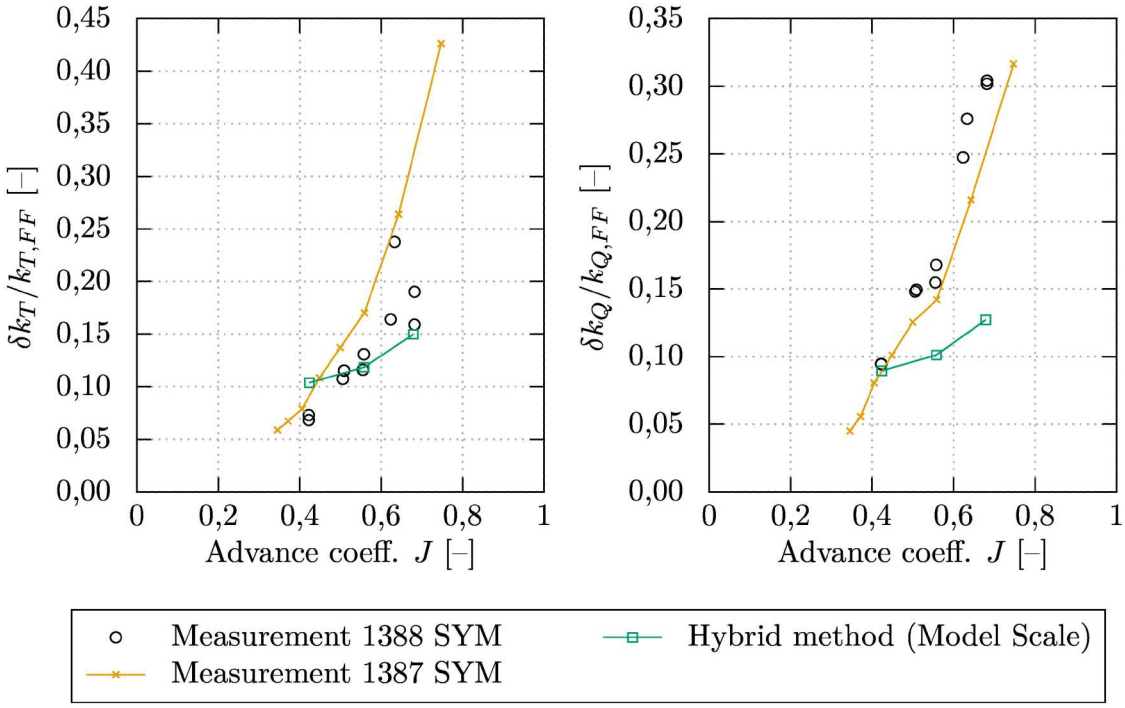

Figure 8. Comparison of relative change in propeller thrust (left) and torque (right) between measurements (Molland and Turnock 1991, 1993) and calculations.

The lift coefficient k_L in Figure 7 is predicted with good accuracy by both calculation methods. At larger positive rudder angles, the hybrid method slightly overestimates the lift. For negative rudder angles, the angle of flow separation seems to be predicted at too small rudder angles. The reason for this could be that already small regions of flow separation occur that do not lead to a sudden drop in lift. Another reason could be that the flow separation is predicted already in the laminar region. A laminar flow separation may reattach after transitioning to turbulent flow. This phenomenon can only partly be investigated with the implemented method. For positive rudder angles, the angle of flow separation is very well predicted.

The drag coefficient k_D in Figure 7 is very close to the results from the measurements and improves the results of Söding (1997). For moderate and larger rudder angles, both calculations deliver a satisfying accuracy up to the flow separation at $|\delta_R| \approx 20°$.

Both calculations overestimate the rudder shaft moment $k_{M,z}$. The attribute of over balance of the rudder is predicted by both methods, but in a too strong manner. The reason for the overestimation is that the investigated rudder is highly balanced, with the absolute shaft moments being very small. Therefore, the deviation of the rudder shaft moment is still in an acceptable range.

The influence of the rudder on the propeller thrust and torque is shown as relative difference of the thrust and torque in propeller–rudder arrangement (index PR) compared to the open water characteristic (index OW) of the propeller:

$$\frac{\delta k_T}{k_{T,\mathrm{OW}}} = \frac{k_{T,\mathrm{PR}} - k_{T,\mathrm{OW}}}{k_{T,\mathrm{OW}}} \tag{4}$$

$$\frac{\delta k_Q}{k_{T,\mathrm{OW}}} = \frac{k_{Q,\mathrm{PR}} - k_{Q,\mathrm{OW}}}{k_{Q,\mathrm{OW}}}. \tag{5}$$

In Figure 8 two measurement series of Wolf (1997) are compared to the results of the hybrid method. The increase of the propeller thrust due to the rudder is predicted with very good accuracy and is within the uncertainty of the measurement. The increase of the propeller torque is predicted with sufficient accuracy. At high advance coefficients the influence is

Figure 9. Rudder and propeller of the validation case of the full scale vessel during construction. Source: Image archive M-06, TUHH.

underestimated. However, it should be noted that the highest calculated advance coefficient is already behind the maximum propeller efficiency, which is not a point of interest in real operating conditions. In this point, the torque already becomes very small, which is why the deviations in relative changes get large.

4. Application to full-scale predictions

The model tests in Section 3.2 were carried out for a vessel that has been built by the FSG[1] in 1997. Using the hybrid method, the results and their scaling to full scale can be further analysed. As the forces and moments were not measured and only can be determined by a large effort on the actual ship in full scale, the full scale prediction itself cannot be validated, but can be checked on plausibility and gives an idea of the potential of the method. In Figure 9, the propeller–rudder arrangement is shown in full scale during construction on the launchway. The full scale dimensions of the rudder are given in Table 2.

4.1. Rudder forces and moments

The forces and moments acting on the rudder are compared in Figure 10 for model and full scale. The

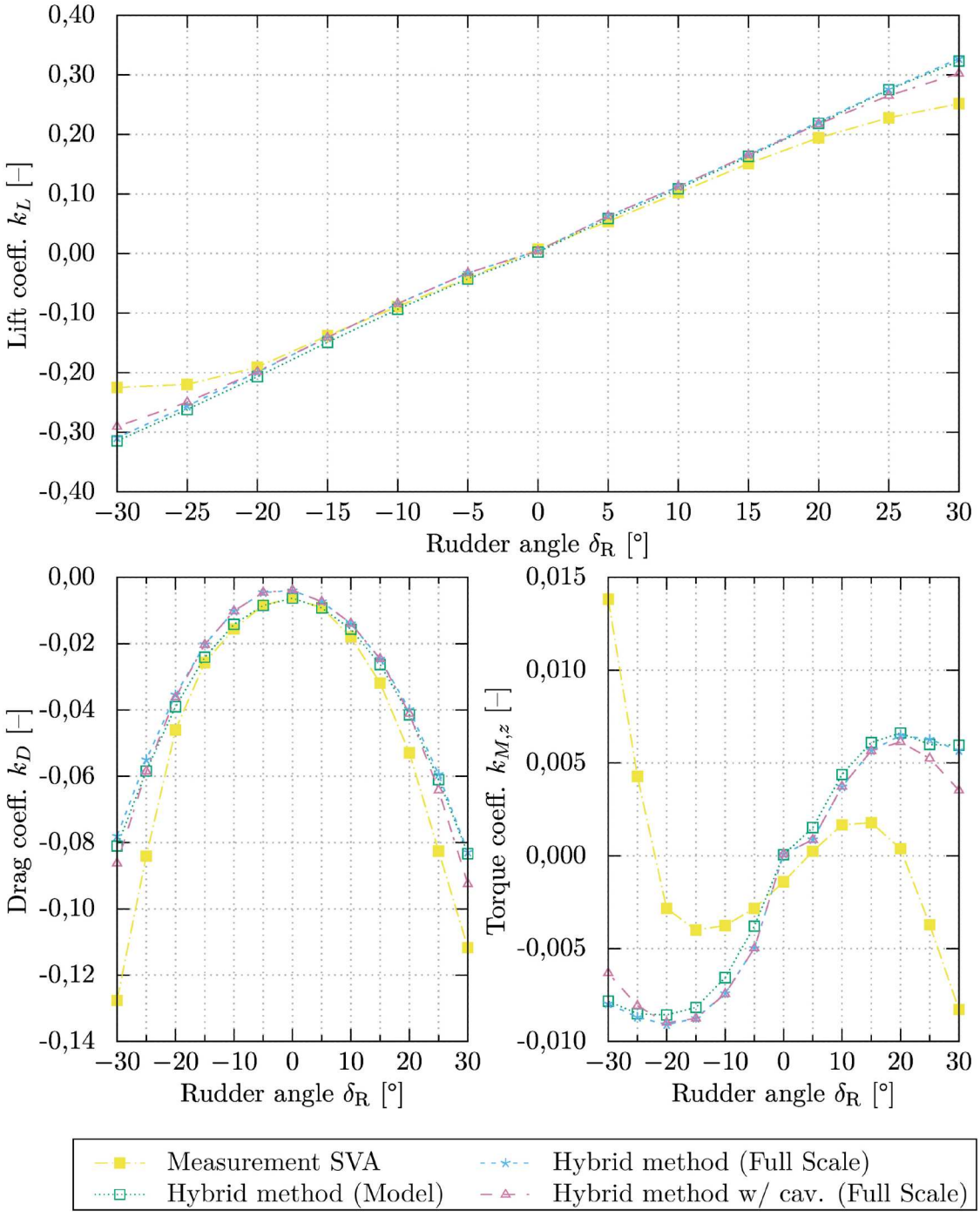

Figure 10. Comparison of rudder forces and torque between calculations with the hybrid method for model scale and full scale (with and without rudder cavitation) and measurements of SVA (Günther and Röpcke 1996).

model test results are given as reference, while the calculations of the hybrid method are shown for model scale, full scale without cavitation and full scale with cavitation.

The lift coefficient k_L and the rudder shaft moment $k_{M,z}$ are only affected marginally by the scale. This corresponds to the expectation, as both values are mainly driven by the potential effect. A minor influence of the onset of cavitation is observed at large rudder angles.

In the full scale prediction, the drag coefficient k_D is calculated lower in full scale than in model scale. For the rudder straight ahead, the drag coefficient in full scale is only 63.2% compared to the drag coefficient in model scale. The absolute offset between the drag coefficient curves of model and full scale stays nearly constant over the rudder angle.

4.2. Trajectories and boundary layer characteristics on the rudder

The trajectories on the rudder surface with the significant points the boundary layer in the two-dimensional computational grid are shown in Figure 11. In the upper row, Figure 11(a,b) show model scale results and the Figure 11(c,d) in the lower row show full scale results. On the left side, the rudder is in straight ahead condition ($\delta_R = 0°$) and on the right side, the rudder is put to $\delta_R = -20°$.

In all sub-figures, the stagnation point (shown in orange) has an S-shape due to the propeller inflow. For the rudder straight ahead ($\delta_R = 0°$), the stagnation point is at the leading edge, while the stagnation point shifts to the star board side when the rudder is put to $\delta_R = -20°$.

According to expectation, the transition point (shown in blue) is further downstream in model scale than in full scale, which can be observed when comparing the condition with rudder straight ahead in Figure 11(a,c). Furthermore, it can be observed in the two sub-figures that the path of the trajectories differs between model and full scale. The reason for this is the different thickness of the boundary layer.

When comparing model and full scale results for the rudder at $\delta_R = -20°$ in Figure 11(b,d), a completely different flow behaviour is observed. In model scale (Figure 11(b)), a laminar separation is found in the lower half on port side near the leading edge (shown in light blue). In full scale, this laminar separation does not occur, but a turbulent separation occurs near the port side trailing edge (marked in red in Figure 11(d)). For this case, the results obtained in model tests cannot be used to make a full scale prediction as the underlying flow pattern is not comparable between model and full scale. The implemented method can identify such operating conditions and thereby show where an analysis with high fidelity full-scale CFD is necessary.

4.3. Change in propeller thrust and torque

The influence of the rudder on the propeller thrust and torque is compared between model and full

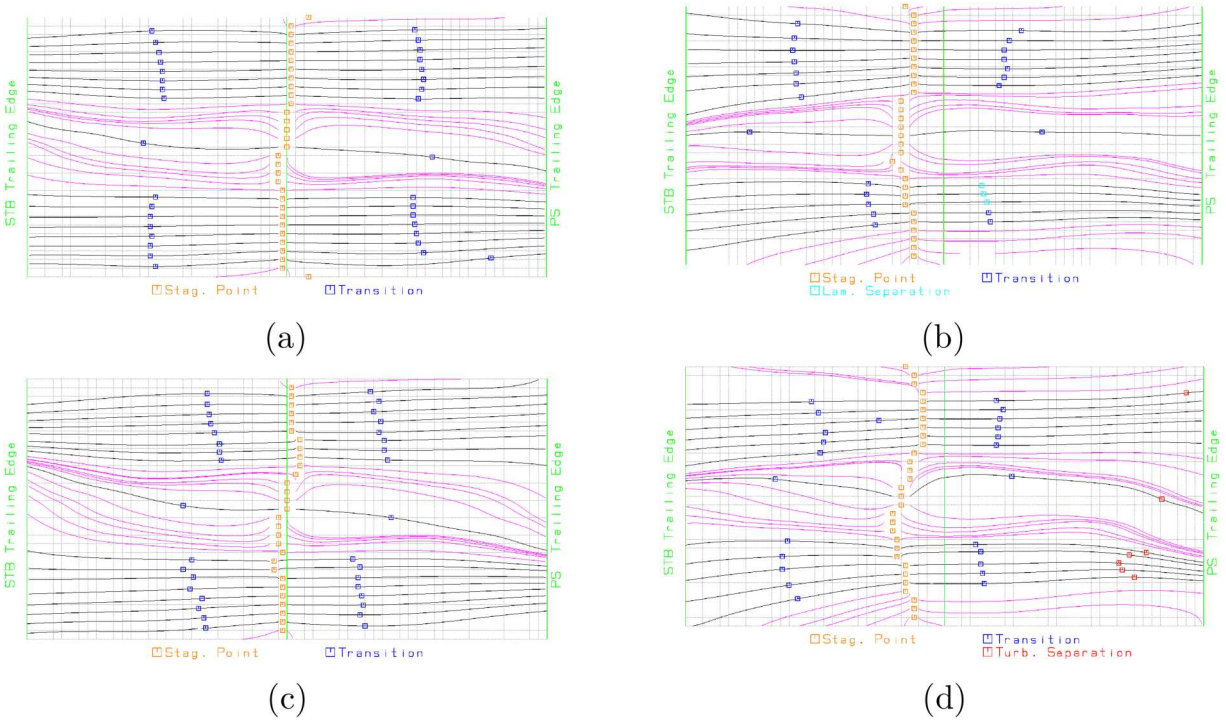

Figure 11. Comparison of trajectories and characteristic points in computational space of the boundary layer method in model scale (top) and full scale (bottom) for rudder angles of $\delta_R = 0°$ (left) and $\delta_R = -20°$ (right) at a thrust coefficient of $c_{TH} = 1.8$. (a) Model Scale, $\delta_R = 0°$. (b) Model Scale, $\delta_R = -20°$. (c) Full Scale, $\delta_R = 0°$. (d) Full Scale, $\delta_R = -20°$.

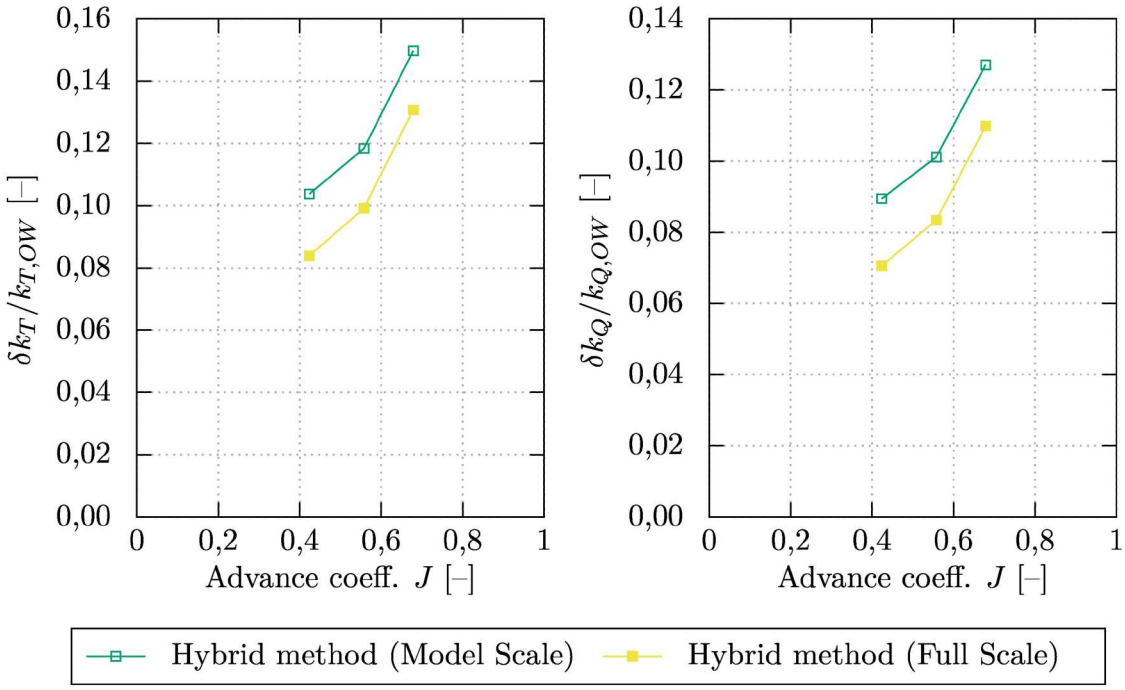

Figure 12. Comparison of relative change in propeller thrust (left) and torque (right) between calculations in model and full scale.

scale in Figure 12. The shown relative difference includes only the effect of the rudder in different scales. The propeller open water characteristics were not scaled. The values of the model scale are the same as already shown in Figure 8. The increase in propeller thrust and torque due to the rudder is by approximately two percentage points lower than in model scale. As the difference in change of propeller thrust and torque is nearly on the same level for this case, the propeller efficiency is only marginally influenced, since the change due to scale cancels out:

$$\eta_O = \frac{J}{2\pi}\frac{k_T}{k_Q}. \tag{6}$$

Nevertheless, the operating condition will slightly change due to the different thrust and torque and by this, the open water efficiency is also affected.

5. Conclusion

The presented newly developed hybrid calculation method improves the accuracy of the rudder force calculation in the early design stage and extends the scope of common procedures. This is achieved while keeping the computation and modelling time on a low level[2] to make the method applicable in the early design stage and for the calculation of numerous operating conditions which subsequently can be used as an input for manoeuvring simulations. The level of detail in the calculations can be adjusted to meet the requirements of the current project stage and the involved party (rudder manufacturer or yard).

The method is validated against the results of several model tests covering different aspects of the application. A good accuracy in forces and moment is reached and the occurrence of flow separation can be investigated. An application of the method is possible in model as well as in full scale. Furthermore, the bidirectional interaction between rudder and propeller is included in the method. In this way, the influence of the propeller inflow on the rudder is captured, but also the upstream influence of the rudder on the propeller, which is needed for a holistic propeller–rudder design.

Notes

1. Flensburger Schiffbau Gesellschaft mbH.
2. Time for grid generation and computation on a single core processor of one operating condition is below one minute for typical amount of iterations when using all presented couplings and extensions.

Acknowledgments

I wish to express my gratitude to the German Federal Ministry of Economic Affairs and Energy for funding and supporting parts of the project. Furthermore, I would like to thank Stefan Krüger for his support and the supervision of my PhD.

Disclosure statement

No potential conflict of interest was reported by the author(s).

Funding

This research was partially sponsored by the German Federal Ministry of Economic Affairs and Energy (formerly BMWi, now BMWK) [grant number 03SX436].

ORCID

Björn Carstensen http://orcid.org/0009-0007-9773-5239.

References

Alte R, vom Baur M. 1986. Propulsion. In: Wendel K, editor. Handbuch der Werften. Schiffahrts-Verlag Hansa; p. 132–211. ISBN 9783877000571.

Carstensen B. 2021. Calculation of rudder forces in the design process using a panel method with a lifting line approach for wake alignment. In: Okada T, Suzuki K, Kawamura Y, editor. Practical design of ships and other floating structures. Springer Singapore; p. 317–330. ISBN 978-981-15-4624-2.

Carstensen B. 2023. Ruderkraftberechnung in der frühen Entwurfsphase unter Berücksichtigung der Propeller-Ruder-Interaktion [dissertation]. Hamburg: TUHH.doi: 10.15480/882.13789

Carstensen B, Krüger S. 2021. Coupling of a boundary element method with a boundary layer method for accurate rudder force calculation within the early design stage. In: 40th International Conference on Ocean, Offshore & Arctic Engineering.

Goldstein S. 1929. On the vortex theory of screw propellers. Proc R Soc Lond Ser A. 123(792):440–465. doi: 10.1098/rspa.1929.0078

Gruschwitz E. 1931. Die turbulente Reibungsschicht in ebener Strömung bei Druckabfall und Druckanstieg. Ingenieur-Archiv. 2(3):321–346. doi: 10.1007/BF02108432ISSN 1432-0681.

Günther B, Röpcke H-J. 1996. Results of resistance an propulsion tests and measurements of the hydrodynamic forces and the torque on rudder with the model of the project C-Box: Bericht 2243. Schiffbau-Versuchsanstalt Potsdam GmbH.

Isay WH. 1964. Propellertheorie : hydrodynamische Probleme. Berlin Heidelberg: Springer (Ingenieurwissenschaftliche Bibliothek). Szabó I., editor.

Isay WH. 1970. Moderne Probleme der Propellertheorie. Berlin Heidelberg: Springer. (Ingenieurwissenschaftliche Bibliothek). Szabó I., editor.

Kringel H. 1974. Berechnung des Fahrtverlustes infolge Wind auf Grund von Winkanal- und Schrägschleppversuchen. Schiff und Hafen. 26(4):343–346.

Krüger S. 1992. Instationäre Grenzschichteffekte an Tragflügelprofilen [dissertation]. Hamburg: Institut für Schiffbau. Universität Hamburg and Technische Universität Hamburg-Harburg.doi: 10.15480/882.960

Krüger S. 2019. Computation of the free vortex system of multi component propulsors. Ship Technol Res. 66(1):1–8. doi: 10.1080/09377255.2018.1500741

Krüger S, Abels W. 2017. Hydrodynamic damping and added mass of modern screw propellers. In: OMAE.

Lerbs H. 1955. Ergebnisse der angewandten Theorie des Schiffspropellers. J Schiffbautech Gesellsch. 46:163–206.

Lighthill MJ. 1958. On displacement thickness. J Fluid Mech. 4(04):383–392. doi: 10.1017/S0022112058000525 ISSN 0022-1120.

Marine Environment Protection Committee. 2011. *Amendments to the Annex of the Protocol of 1997 to Amend the International Convention for the Prevention of Pollution from Ships, 1973, as Modified by the Protocol of 1978 Relation Thereto: Resolution MEPC.203(62).*

Marine Environment Protection Committee. 2018. *Initial IMO strategy on reduction of GHG emissions from ships: Resolution MEPC.304(72).*

Marine Environment Protection Committee. 2021. *Amendments to the Annex of the Protocol of 1997 to Amend the International Convention for the Prevention of Pollution from Ships, 1973, as Modified by the Protocol of 1978 Relating Thereto: Resolution MEPC.328(76).*

Marzi J. 1988. Ein Berechnungsverfahren zur Behandlung von Profilströmungen mit lokalen Ablösezonen und offenen Totwassergebieten. TUHH Universitätsbibliothek. No. 3-89220-481-0. Available from doi: 10.15480/882.899

Molland AF, Turnock SR. 1991. Wind tunnel investigation of the influence of propeller loading on ship rudder performance [Tech. rep., 46]. University of Southampton. ISSN 0140-3818.

Molland AF, Turnock SR. 1993. Wind tunnel tests on the influence of zero speed operation [Tech. rep., 64]. University of Southampton. ISSN 0140-3818.

Molland AF, Turnock SR. 2007. Marine rudders and control surfaces: principles, data, design and applications. Amsterdam:Butterworth-Heinemann.

Orr WM'F. 1907. The stability or instability of the steady motions of a perfect liquid and of a viscous liquid. part II: A viscous liquid. Proc R Irish Acad Sect A. 27:69–138. [accessed 2025 May 5]. ISSN 00358975. http://www.jstor.org/stable/20490591.

Pohlhausen K. 1921. Zur näherungsweisen Integration der Differentialgleichung der laminaren Grenzschicht. J Appl Math Mech. 1(4):252–290. ISSN 00442267.

Simonsen CD. 2000. Rudder, propeller and hull interaction by RANS [PhD thesis]. Lyngby: Department of Naval Architecture and Offshore Engineering. Technical University of Denmark.

Söding H. 1997. Limits of potential theory in rudder flow prediction. Ship Technol Res. 45(3):141–155.

Sommerfeld A. 1908. Ein beitrag zur hydrodynamischen Erklärung der turbulenten Flüssigkeitsbewegungen. In: Proceedings of the 4th International Congress of Mathematicians III, 116ñ124.

Squire HB, Young BA. 1937. The calculation of the profile drag of aerofoils. In: Aeronautical Research Committee Reports and Memoranda, p. 1838.

Turnock SR. 1993. Prediction of ship rudder-propeller interaction using parallel computations and wind tunnel measurements [PhD thesis]. Southampton: Faculty of Engineering and Applied Science. University of Southampton.

von Kármán T. 1921. Über laminare und turbulente Reibung. J Appl Math Mech. 1(4):233–252. ISSN 00442267. Engl. translation in: 'On laminar and turbulent friction'. NACA-TM–1092.

Wagner B. 1974. Zur Frage des effektiven Zusatzwiderstandes durch den Wind auf der Grundlage von Modellversuchen für Unter- und Überwasserschiffe. Schiff und Hafen. 26(3):259–266.

Wolf E. 1997. Untersuchung von Twist-Flow-Ruderformen im Propellerstrahl [Diplomarbeit]. Kiel: Institut für Schiffbau. FH Kiel.

Zingg DW, Yarrow M. 1989. A direct procedure for interpolation on a structured curvilinear two-dimensional grid [Tech. rep., 102213]. California: NASA.